Molecular Imaging Application of Radioiodinated Anti-EGFR Human Fab to EGFR-overexpressing Tumor Xenografts

NING XU[1], GANGMING CAI[2], WANZHONG YE[2], XIN WANG[3], YUNQIAN LI[1], PING ZHAO[4], AIXIA ZHANG[1], RONGJUN ZHANG[2] and BRIAN CAO[1,4]

[1]*Cancer Center, Key Laboratory of Antibody Technology of Ministry of Health, Nanjing Medical University, Nanjing, Jiangsu 210029;*
[2]*Key Laboratory of Nuclear Medicine, Ministry of Health, Jiangsu Institute of Nuclear Medicine, Wuxi, Jiangsu 214063;*
[3]*Department of Endocrinology, Jiangsu Province Hospital of Traditional Chinese Medicine, Nanjing, Jiangsu 210029, P.R. China;*
[4]*Antibody Technology Laboratory, Van Andel Research Institute, Grand Rapids, MI 49503, U.S.A.*

Abstract. *Background: Suitable diagnostics could identify patients who might benefit from targeted therapies. Molecular imaging is a promising method estimating the expression of specific molecules in vivo, and the goal of this study was to evaluate a radioiodinated anti-epidermal growth factor receptor (EGFR) human Fab as a molecular imaging agent for diagnosis. Materials and Methods: Three human tumor cell lines representing tumors with different levels of EGFR expression were selected and their corresponding xenografts produced. ^{125}I was conjugated to a human anti-EGFR Fab that recognizes the native extracellular domain of EGFR evidenced by immunoprecipitation (IP) and fluorescence-activated cell sorting (FACS) assays. Single-photon-emission computed tomography (SPECT) imaging of ^{125}I-Fab being administered to nude mice bearing xenografts were obtained, and further analyzed by region of interest (ROI) assay. Results: The ^{125}I-Fab was achieved successfully without losing its immunoreactivity. The scintigrams as well as ROI assay showed that ^{125}I-Fab was able to clearly quantitatively distinguish the different expression levels of EGFR in vivo. Conclusion: ^{125}I-Fab is a potential molecular imaging agent for clinical diagnosis of EGFR-overexpressing tumors.*

Correspondence to: B. Cao, Van Andel Institute, 333 Bostwick Ave. N.E, Grand Rapids, MI 49503, U.S.A. Tel: +1 6162345342, e-mail: brian.cao@vai.org; R.J. Zhang, Key Laboratory of Nuclear Medicine, Ministry of Health, Jiangsu Institute of Nuclear Medicine, 20 Qianrong Road, Wuxi, Jiangsu 214063, P.R. China. Tel: +86 13951587106, e-mail: zrhj@yahoo.com

Key Words: Anti-EGFR Fab, molecular imaging, ^{125}I.

The epidermal growth factor receptor (EGFR; ErbB1) belongs to the tyrosine kinase receptor family that also includes ErbB2, ErbB3, and ErbB4 (1). When activated by binding with its ligands, EGFR initiates a signaling cascade leading to cell proliferation, differentiation, or repair (2). Dysregulation of EGFR signaling has emerged as a crucial feature of many human malignancies, including cancer of breast, lung, and head and neck, as well as glioblastoma and colorectal, ovarian, and prostate cancer (3). Numerous studies have shown a correlation between EGFR overexpression and tumor growth, angiogenesis, invasion, metastasis, and apoptosis inhibition (4). Clinical data have also confirmed that increased EGFR expression is associated with more aggressive disease, resistance to chemotherapy and radiotherapy, and poor prognosis and survival (5). The role of EGFR in carcinogenesis and its localization on the cell surface as a transmembrane protein make it an ideal target for cancer immunotherapy (6).

Targeted therapy may only benefit patients who have a tumor overexpressing the targeted molecule, so determining the expression level of the specific molecule is a crucial step before treatment. Currently, the most commonly used method for detecting EGFR levels is staining by immunohistochemistry (IHC), which has been applied in the majority of published studies. However, there are considerable variations between laboratories in the execution of this method in terms of application of reagents and even differences in the definitions used for high expression or overexpression (7). Therefore, the evaluation of EGFR level by IHC might not be the best method for screening patients before targeted treatment.

Medical imaging technologies have undergone enormous growth over the past decades and now play an important role in clinical oncology. Molecular imaging with single-photon-emission computed tomography (SPECT) and

positron-emission tomography (PET) has been considered one of the most promising ways to show molecular expression more directly and exactly than traditional IHC can do (8). This method determines tumor location accurately, visualizing the expression and activity of a specific target non-invasively, and reflecting tumor response to therapy. Some monoclonal antibodies (mAbs) coupled with various radionuclides have been used in clinical imaging diagnosis (9, 10). However, the disadvantages of IgG, such as long halflife, poor penetration, and immunogenicity of murine origin, have limited the application of this method. Human (or humanized) antibody fragments such as Fab are considered to be more suitable agents for molecular imaging diagnosis.

We previously generated a fully human anti-EGFR Fab that recognizes the extracellular domain of EGFR in native conformation (11). In this study, we radioiodinated this Fab and evaluated its ability to identify tumors having different EGFR expression levels in xenograft models.

Materials and Methods

Reagents, antibodies and cell lines. ^{125}I was purchased as NaI from Chengdu Gaotong Corp. (Chengdu, Sichuan, PRC). All other reagents were of the best commercial grade available. The human anti-EGFR Fab fragment was previously generated in our lab (11). The cell lines used in this research were A431 (human epidermoid carcinoma overexpressing EGFR), NIH 3T3 (EGFR-negative mouse fibroblast), U118 and U87 (human glioma), M14 (human melanoma), and MCF-7 (human breast carcinoma). Cells were maintained in DMEM (#11965 092; Gibco, Carlsbad, CA, USA) containing 10% fetal bovine serum.

Reverse transcription–polymerase chain reaction (RT-PCR). The RNA was collected from cultured cells using Trizol (#15596-026; Invitrogen, Carlsbad, CA, USA). The total RNA was reverse-transcribed in a 20-μl reaction mixture (#28025-013; Invitrogen), and the resultant cDNA was amplified by PCR (#EP0404; Fermentas, Burlington, Ontario, Canada) in a 25-μl volume. The primer (5'-3') sequences specific for human EGFR were as follows: GGACGACGTGGTGGATGCCG (forward) and GGCGCCTGT GGGGTCTGAGC (reverse). The PCR program used here was initial denaturation at 94˚C for 4 min, followed by 30 cycles at 94˚C for 45 s, 60˚C for 60 s, 72˚C for 60 s. After a final extension at 72˚C for 10 min, the PCR products were run on a 1% agarose gel with a 2,000-bp DNA marker (#D501A; TaKaRa, Otsu, Shiga, Japan).

Western blot. Cells were lysed in RIPA cell lysis buffer (1% NP-40, 1% sodium deoxycholate, 1% SDS, 0.15 M NaCl, 2 mM EDTA, and 50 mM NaF at pH 7.2, 10 mM phosphate buffer), and the protein concentration of lysates were quantified by BCA assay (#23227; Pierce, Rockford, IL, USA). Normalized aliquots of cell lysates were loaded onto 10% SDS-PAGE gels for electrophoresis and transferred onto polyvinylidene difluoride (PVDF) membrane. Proteins were detected using rabbit anti-EGFR polyAb (#sc-07; Santa Cruz, Santa Cruz, CA, USA) and anti-β-actin mAb as a loading control (#BM0627; Boster, Wuhan, Hubei, PRC).

Fluorescence-activated cell sorting (FACS) analysis. A431, NIH 3T3, M14, and U118 cells (1×10^6 each) were detached by TrypLE Express (#12605-028; Invitrogen) and blocked in 5% milk at 4˚C for 30 min. Cells were incubated with anti-EGFR Fab at a final concentration of 100 μg/ml for 60 min at 4˚C and then stained using 1:25 diluted fluorescein isothiocyanate (FITC) labeled anti-human Fab IgG (#F5512; Sigma, St. Louis, MO, USA) for 30 min at 4˚C. The cells were washed twice and suspended in 500 μl phosphate-buffered saline (PBS). Fluorescence intensity was analyzed by the flow cytometer (BD Bioscience, San Jose, CA, USA). Cells incubated with secondary antibody only were analyzed as controls.

Immunoprecipitation (IP). Each cell lysate of A431, NIH 3T3, M14, and U118 (600 μg each) in RIPA cell lysis buffer was mixed with 25 μg anti-EGFR Fab and 30 μl Protein G Agarose beads (#15920-010; Invitrogen) at 4˚C overnight. The beads were washed three times with 0.1% Tween-PBS and resuspended in 30 μl 2×SDS loading buffer, heated at 100˚C for 10 min, and centrifuged at 5,000 × g for 5 min. The supernatant was then collected for Western blotting to detect the precipitated EGFR.

Radioiodination of anti-EGFR Fab. Fab was radioiodinated by the procedure described elsewhere (12). Briefly, 10 μg Fab in 20 μl of 0.2 M phosphate buffer (pH 8.0) were added to 74 MBq (2.0 mCi; 6.0 μl) of ^{125}I as sodium iodide and 10 μl (3 mg/ml) of chloramine T. The reactants were mixed and agitated gently for 60 s at room temperature. The reaction was quenched by the addition of 20 μl (5 mg/ml) of sodium metabisulfite. ^{125}I-Fab was separated from nonreacted ^{125}I on a PD-10 desalting column (#17-0851-01; GE, Niskayuna, NY, USA). The labeling efficiency was determined in a Perkin Elmer 1470 Automatic Gamma counter (Fremont, CA, USA), and the radiochemical purity of ^{125}I-Fab was assessed by a trichloracetic acid (TCA) assay as described elsewhere (13).

Immunoreactivity assay. The immunoreactivity of the radioiodinated Fab was compared with unlabeled Fab by enzyme linked immunosorbent assay (ELISA). Briefly, enzyme-immunoassay (EIA) plates were coated with recombinant human EGFR protein at 0.5μg/ml (#1095-ER-002; R&D, Minneapolis, MN, USA). The ^{125}I-Fab and unlabeled Fab were equally diluted (twofold series) starting at 12.5 μg/ml, and then were incubated with coated plates in triplicate at 37˚C for 60 min. The plates were washed 4 times and then horseradish peroxidase (HRP)-conjugated anti-human Fab IgG with the dilution of 1:2,000 was added for another 60 min at 37˚C. Finally, HRP substrate was added for 30 min and then the reaction was stopped by addition of 1 M H_2SO_4; the absorbance value was read at 450 nm (Multiskan Spectrum; Thermo, Rockford, IL, USA).

To determine whether the immunoreactivity of ^{125}I-Fab can be demonstrated by γ rays from the conjugated ^{125}I, ^{125}I-Fab at the same concentrations described above was incubated with the coated plates. After incubation at 37˚C for 90 min, the plates were washed once and read directly by the gamma reader. A mixture of unlabeled Fab and ^{125}I-Fab in a molar ratio of 200:1 was incubated with plates as negative control. This assay was repeated three times and the results were analyzed by *t*-test.

In vitro cell uptake assay of ^{125}I-Fab. A431, NIH 3T3, and U118 cells (2×10^6 each) were suspended in 0.2% BSA-PBS and split into two groups. One group was incubated with ^{125}I-Fab at a final concentration of 3μg/ml for 1 h in a 37˚C water-bath. Cells were

washed twice and spun at 3,000 rpm for 10 min. The radioactivity of the pellets was then read by the gamma reader. Another group of cells was incubated with 3 μg/ml of labeled Fab in the presence of 200-fold unlabeled Fab to determine the nonspecific binding.

Xenograft model and in vivo imaging. All studies involving animals were conducted in compliance with the state and university's animal care guidelines. Female athymic nude (*nu/nu*) mice at 6 weeks of age received *s.c*. injections of tumor cell suspensions in the right forelimbs. The mice were housed in small groups and given food and water *ad libitum*. Drinking water contained 0.1% potassium iodide to block thyroid uptake of iodine. Tumors reached ≥1.0 cm in greatest dimension by external caliper measurement before imaging.

Animals were imaged and scintigrams were analyzed by previously established methods (12). In brief, each mouse received 11.1 MBq (300 μCi) ^{125}I-Fab, representing 3 μg of protein, in 150 μl PBS (0.2% BSA) by tail vein injection under light inhalation anesthesia. Prior to the imaging session, each mouse was given up to 13 mg/kg xylazine and 87 mg/kg ketamine *s.c*. in the interscapular region. Sedated mice were placed face down singly or in pairs at optimum limb extension. Whole-body images of each mouse were acquired at 2, 4, 9, 15, 18, and 24 h post-injection by SPECT (Skylight; Philip, Amsterdam, the Netherlands). Computer-assisted region of interest (ROI) were drawn around the tumor and in the contralateral region located in the left forelimb (background) to achieve the corresponding values at different imaging time points. The specific uptake of ^{125}I-Fab in the tumors was estimated by the ratio of values from tumor regions to those from contralateral normal regions, designated as the T/N ratio.

Results

Selection of tumor cell lines having different EGFR expression levels. To select the tumor cell lines having high, moderate, or low EGFR expression, we analyzed the *EGFR* mRNA and protein levels in 6 cell lines: A431, U118, U87, MCF-7, M14, and NIH 3T3. As a positive control, A431 is a well-known EGFR-overexpressing cell line, with about 2.6×10^6 EGFR molecules per cell (14). *EGFR* mRNA was detected by RT-PCR; all cell lines showed almost the same level of EGFR expression except the positive (A431) and negative (NIH 3T3) controls (Figure 1A). However, the protein expression levels differed dramatically in comparison to the mRNA result. Only U118 and U87 exhibited moderate EGFR abundance, while it was undetectable in both MCF-7 and M14 cells; A431 still showed the highest abundance (Figure 1B). We therefore selected A431, U118, and M14, representing high, moderate, and low EGFR expression, for molecular imaging experiments.

Evaluation of human anti-EGFR Fab binding to native EGFR. To determine whether the human anti-EGFR Fab recognizes EGFR in native conformation on the tumor cells, IP assays were performed with A431, U118, M14, and NIH 3T3 cells. The results showed that the Fab was able to bind EGFR from the A431 and U118 cell lysates but not from M14 and NIH 3T3 lysates (Figure 2A). The precipitated

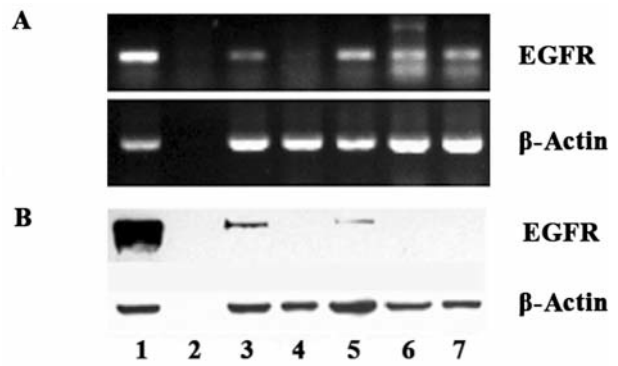

Figure 1. *RT-PCR and Western blot characterization of EGFR expression at mRNA and protein level respectively in different human tumor cell lines. A, RT-PCR: The total RNA from each cell line was reverse-transcribed and amplified as the template. B, Western blot: Thirty micrograms of each cell lysate were loaded. Lane 1, A431; Lane 2, blank; Lane 3, U118; Lane 4, NIH3T3; Lane 5, U87; Lane 6, MCF-7; Lane 7, M14.*

EGFR from U118 was less than that from the positive control A431, which correlated with the Western blotting result. In addition, Fab-specific binding to native EGFR was evaluated by flow cytometric assay. Fab-treated A431 and U118 cells were clearly separated from non-treated cells but M14 and NIH 3T3 cells were not. Furthermore, the fluorescence intensity also distinguished the different expression levels of EGFR. The FACS result showed good consistency with IP and Western blotting analyses (Figure 2B). In conclusion, both IP and FACS data demonstrated that the Fab bound the extracellular domain of EGFR in native conformation.

Radioiodination of anti-EGFR Fab and in vitro immunoreactivity assay. The radioiodination labeling efficiency was about 75% assuming complete recovery of Fab from the labeling mixture, and the radiochemical purity was above 95% . To evaluate the immunoreactivity change after the labeling reaction, we performed an ELISA assay with ^{125}I-Fab and unlabeled Fab at the same concentration to compare the resultant OD_{450} absorbance values. The ELISA data showed that the reactivity of ^{125}I-Fab to EGFR was decreased to 62.97% that of the unlabeled Fab value (Figure 3); in other words, the radioiodinated Fab was still able to recognize EGFR specifically. We further tested the capability of ^{125}I-Fab binding to EGFR by gamma counting. The cpm values from the wells incubated with ^{125}I-Fab were significantly higher than those containing the negative control ($p<0.01$, data not shown), suggesting that ^{125}I-Fab binding capacity could also be quantitatively measured by radioactivity counting.

To determine whether the labeled Fab recognizes EGFR in native conformation on cell surfaces, we performed a cell uptake assay. The cpm values of ^{125}I-Fab bound to A431 and

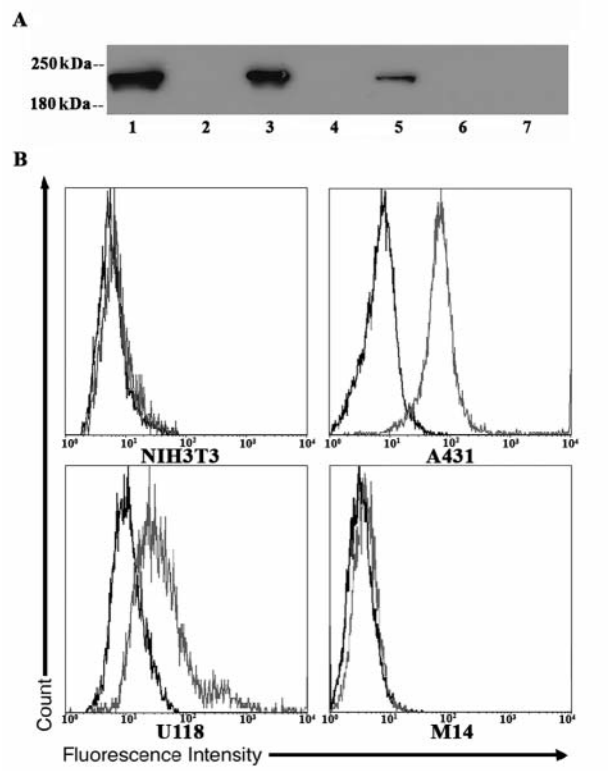

Figure 2. *The anti-EGFR Fab recognized the EGFR extracellular domain in native conformation. A, Immunoprecipitation: lane 1, 20 μg of A431 cell lysate loaded directly as a positive control; lane 2, RIPA buffer only as a blank for immunoblotting; lane 3 to lane 6, 600 μg each of A431, NIH 3T3, U118, and M14 cell lysates immunoprecipitated with 25 μg anti-EGFR Fab and 30 μl protein-G beads respectively; lane 7 was RIPA buffer, Fab, and beads. All samples were subjected to immunoblotting with rabbit-anti-EGFR antibody followed by goat anti-rabbit HRP conjugate. B, Flow cytometric analysis: the Fab-treated A431 and U118 cells were clearly separated from non-treated cells but not in the case of M14 and NIH 3T3 cells. The fluorescence intensity also distinguished the different expression levels of EGFR. Grey line: population of cells treated with Fab and anti-Fab IgG-FITC; black line: population of cells treated with anti-Fab IgG-FITC only.*

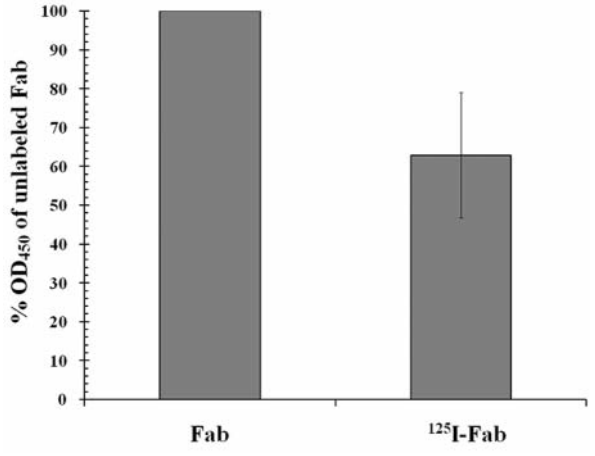

Figure 3. *Estimation of the immunoreactivity alteration of the ^{125}I-Fab by ELISA. The labeled and unlabeled Fabs at the same concentration were incubated on EGFR protein-coated plates in six parallel twofold dilutions. Anti-Fab IgG-HRP was added and followed by HRP substrate to test the absorbance at 450 nm (OD_{450}) of the two groups. The OD_{450} of labeled Fab was decreased to 62.97% relative to that of unlabeled Fab.*

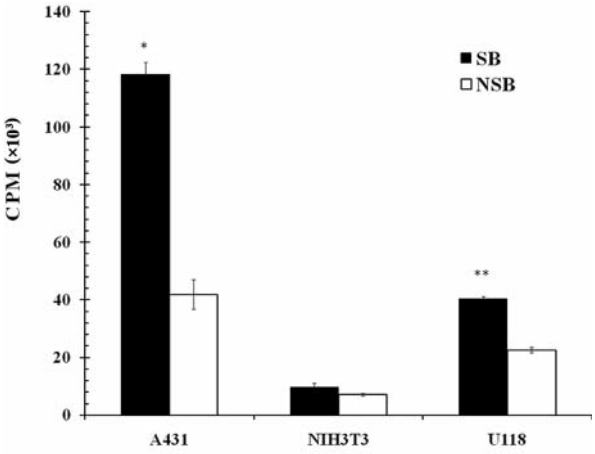

Figure 4. *Cell uptake assay of ^{125}I-Fab. A431, NIH3T3, and U118 cells were separately incubated with ^{125}I-Fab (designated as SB, specific binding) at a final concentration of 3 μg/ml for 1 h in a 37°C water-bath, then were read by a gamma reader and shown as counts per minute (cpm). Cells were incubated with 3 μg/ml of ^{125}I-Fab in the presence of a 200-fold molar excess of unlabeled Fab, determining the nonspecific binding as the blank (NSB, nonspecific binding). The ^{125}I-Fab was only taken up by the EGFR-expressing cells A431and U118 specifically (*p<0.01, **p<0.05, SB vs. NSB), and not by the negative control, NIH3T3.*

U118 cells were 3- and 2-fold greater, respectively, than the values for NIH 3T3 cells (Figure 4, black bars). The binding of ^{125}I-Fab to the A431 and U118 cells was EGFR-specific, as evidenced by blocking with excess of unlabeled Fab (white bars, A431: $p<0.01$; U118: $p<0.05$ *vs.* unblocked values); the blocked and unblocked values were not statistically different for NIH 3T3 cells as a negative control.

In vivo imaging. Serial, whole-body gamma camera images were acquired for individual mice bearing human cancer xenografts having different EGFR expression levels from three tumor origins (A431, U118, and M14). Images were taken within 24 h following *i.v.* injection of ^{125}I-Fab. The activity was evident in the A431 xenograft as early as 1 h post-injection and prominently thereafter. Tumor uptake was also clearly seen in U118 tumors expressing moderate EGFR. Mice bearing M14 tumors (low EGFR level) showed

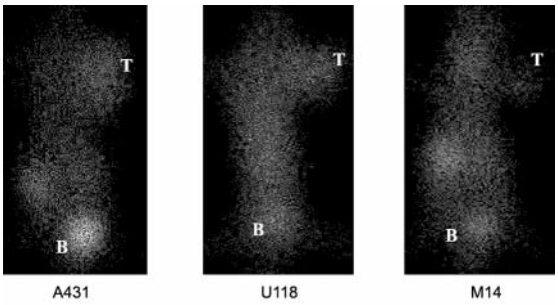

Figure 5. *Scintigrams were obtained at 9 h post-injection of ^{125}I-Fab. The radioactivity was prominent in the A431 xenograft expressing a high EGFR level and also seen in U118 tumors expressing moderate EGFR. Mice bearing M14 tumors (low EGFR level) showed very low uptake in the xenograft that rapidly decreased within 9 h; T: xenograft; B: bladder.*

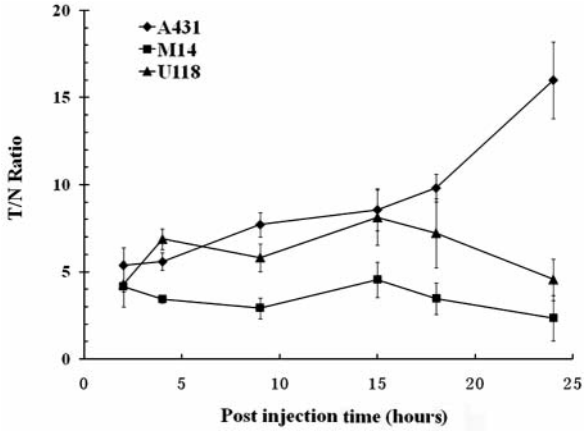

Figure 6. *The tumor-specific uptake of ^{125}I-Fab. To quantify tumor specific uptake of the conjugate, the scintigrams at six post-injection time points were analyzed by ROI assay and uptake estimated by the ratio of tumor regions to contralateral normal regions, designated as the T/N ratio. The T/N ratio increased significantly in A431, and in U118 (representing moderate EGFR expression) tumors; it also increased with the same trend in U118 tumors before reaching a lower peak at 15 h post-injection. As for M14 (low EGFR expression), no significant ratio changes were identified.*

nonspecific uptake in the xenograft that rapidly decreased within 4 h. At 9 h post-injection, the activity in the A431 and U118 tumors became more evident, while that in the M14 tumor disappeared as the radioactivity in circulation was eliminated (Figure 5).

To quantitatively analyze these apparent differences, we examined the images at six post-injection time points by ROI analysis (Figure 6). The ratio of tumor regions to contralateral normal regions (T/N ratio) increased significantly in A431 as time went on, reaching a peak 48 h post-injection (data not shown). The T/N ratio of U118 (moderate EGFR expression) also increased with the same trend as for A431, before reaching its lower peak at 15 h post-injection. No significant T/N ratio changes were identified in the M14 tumor models. The higher the T/N ratio, the more specific ^{125}I-Fab was taken up by the tumor.

These data showed that ^{125}I-Fab was not only able to specifically detect the EGFR-overexpressing tumors *in vivo*, but also differentiate the high, moderate, and low EGFR expression levels of the tumors. This capability suggests that ^{125}I-Fab is a potential clinical diagnostic agent for molecular imaging of selected patients who might benefit from EGFR-targeted therapy.

Discussion

The rationale for selecting EGFR as a target for cancer therapy was based on its overexpression in many different human tumors and its association with aggressive disease and poor prognosis. EGFR-targeting agents have been introduced and achieved encouraging therapeutic effects in clinical trials (15). In theory, the EGFR status of a tumor indicates the likelihood of response to EGFR-targeted therapy. However, the clinical data do not always support this relationship (16). One possible explanation for this inconsistency is the absence of a sensitive and standardized EGFR detection method. The most commonly used method is IHC, but because of the diversity in application of the reagents, protocol methods, and assessment standards from different trained pathologists of various laboratories and hospitals, the determinations made by IHC are not always reproducible and comparable. Molecular imaging is the integration of molecular and physiological information specific to each patient, and as a non-invasive method, could be used to monitor the patient's response to a targeted treatment during the therapy, which might be accordingly adjusted in real time.

The goal of this study was to develop a diagnostic agent of radiolabeled anti-EGFR Fab and to evaluate EGFR expression on various tumors before targeted treatment. A number of studies have been undertaken with radionuclide-labeled monoclonal antibodies targeting EGFR (10, 17), and some disadvantages have appeared. Large molecules such as IgG (150 kDa) have a limited capability for penetrating a tumor, and their halflife in the blood is long, resulting in a high background upon image acquisition and low T/N ratios (18). Therefore, the use of smaller antibody fragments such as Fab (50 kDa) could be an advantage (19, 20). In this study, the anti-EGFR Fab was selected from a large human naïve Fab phage library (21), having an affinity of 30 nM. This Fab also recognized native EGFR on various tumor cells, as evidenced by the IP and FACS results, which made it a suitable agent for the molecular imaging of cancer.

Recently, several radiolabeled small molecules targeting EGFR have been reported, including the EGFR-specific Affibody molecules (22) and a llama single-domain antibody fragment termed Nanobody (23). They all had achieved good tumor-to-organ ratios *in vivo*, but they failed to correlate tumor uptake with EGFR expression. In this study, we established xenograft models of A431, U118, and M14 cells representing high, moderate, and low EGFR expression. The ^{125}I-Fab bound the receptor specifically, and the tumors expressing high or moderate EGFR could be imaged. As time went on, the signals of background decreased rapidly and the tumor images of A431 became more prominent than that of U118 even 24 h post-injection. In order to analyze the different expression levels of EGFR quantitatively, the ROI assay was performed. The T/N ratio of A431 tumors kept increasing until it reached a peak at 48 h post-injection. U118 tumors showed the same trend except that the peak was lower and appeared earlier, at 15 h, while M14 tumors showed no significant ratio changes. It remains unclear why the T/N ratio of A431 tumors stayed at a high level and for a much longer time than it did for U118 tumors (48 h *vs*. 15 h). A possible explanation is that this anti-EGFR Fab was able to be taken into the cytosol of EGFR-positive cells through receptor binding (11), and A431 cells have the highest level of EGFR, resulting in more ^{125}I-Fab accumulation inside the tumor cells. Moreover, we also used 2-[^{18}F]fluoro-2-deoxy-D-glucose (FDG), the most useful probe for tumor imaging by micro-PET, to image the same tumors. All tumors were clearly imaged, but no differences were identified among the different EGFR levels (data not shown). Only EGFR-specific ^{125}I-Fab was able to discriminate among the tumors having various EGFR expression levels.

EGFR was overexpressed on a variety of tumor cells but was also present on some normal cell types such as epithelium (19), though the expression level was too low to be detected by Western blotting. Our imaging results demonstrated that the ^{125}I-Fab did not accumulate in the M14 tumor cells (low EGFR expression), in which the EGFR expression level was comparable with normal epithelial cells. Because of this threshold effect, the ^{125}I-Fab could be a more ideal agent in molecular imaging to distinguish between the different EGFR-expressing tumors in individual patients and to identify those who may benefit by EGFR-targeting therapy.

However, as a proof-of-concept study, these preliminary results were obtained only from xenografts of three tumor origins representing different EGFR expression levels; further studies are needed to image animals with more tumor cell lines, and the body distribution of ^{125}I-Fab at different time points should also be analyzed. Additionally, all the mice were imaged by clinical SPECT, which is not specific for small animals, resulting in the scintigram resolution being relatively low; however, the ^{125}I-Fab accumulation in EGFR-overexpressing xenografts was still evident. Moreover the affinity is another important factor, helping reach a higher peak of T/N ratio within shorter time. The affinity of our Fab targeting EGFR is about 30 nM (11), and a Fab of higher affinity is currently under development to achieve better imaging *in vivo*.

Another application of radionuclide-conjugated antibodies is radioimmunotherapy (RIT), and ^{131}I is widely used in this field. ^{131}I decays by both β and γ emission, and β-particle emitters are proved to be good cytotoxic agents, having a relatively long penetration range with higher energy (about 3- to 10-fold higher than ^{125}I) (24). Both ^{131}I and ^{125}I belong to the radioiodine family and share similar chemical characteristics, so that they can be modified by an oxidant such as chloramine-T when conjugated to antibodies, and similar labeling efficacies may be achieved. We suggest that this Fab can be radioiodinated with ^{131}I instead of ^{125}I, making it a potential therapeutic agent for treating EGFR-overexpressing tumors, because this Fab not only binds to the EGFR extracellular domain but is also internalized through receptor binding.

In summary, we characterized six human tumor cell lines having different levels of EGFR expression, and we selected A431, U118, and M14 for a molecular imaging study with fully human anti-EGFR ^{125}I-Fab. The ^{125}I-Fab had reasonable antigen-binding capability and accumulated only in tumors with high or moderate EGFR expression. Moreover, it was possible to use the acquired scintigrams to measure EGFR density on the tumors, making it a potential agent for imaging diagnosis of EGFR-overexpressing tumors.

Acknowledgements

We thank David Nadziejka for editorial reading of the manuscript. This work was partially supported by Jiangsu Province's Key Medical Talents Program (No. RC2007097).

References

1 Yarden Y and Sliwkowski MX: Untangling the ErbB signalling network. Nat Rev Mol Cell Biol *2*: 127-137, 2001.

2 Olayioye MA, Neve RM, Lane HA and Hynes NE: TheErbB signaling network: receptor heterodimerization in development and cancer. EMBO J *19*: 3159-3567, 2000.

3 Mendelsohn J and Baselga J: Status of epidermal growth factor receptor antagonists in the biology and treatment of cancer. J Clin Oncol *21*: 2787-2799, 2003.

4 Ciardiello F and Tortora G: A novel approach in the treatment of cancer: targeting the epidermal growth factor receptor. Clin Cancer Res *7*: 2958-2970, 2001.

5 Ang KK, Berkey BA, Tu X, Zhang HZ, Katz R, Hammond EH, Fu KK and Milas L: Impact of epidermal growth factor receptor expression on survival and pattern of relapse in patients with advanced head and neck carcinoma. Cancer Res *62*: 7350-7356, 2002.

6 Reusch U, Sundaram M, Davol PA, Olson SD, Davis JB, Demel K, Nissim J, Rathore R, Liu PY and Lum LG: Anti-CD3 x anti-epidermal growth factor receptor (EGFR) bispecific antibody redirects T-cell cytolytic activity to EGFR-positive cancers *in vitro* and in an animal model. Clin Cancer Res *12*: 183-190, 2006.

7 Meropol NJ: Epidermal growth factor receptor inhibitors in colorectal cancer: it's time to get back on target. J Clin Oncol *23*: 1791-1793, 2005.

8 Weissleder R: Molecular imaging in cancer. Science *312*: 1168-1171, 2006.

9 Reilly RM, Kiarash R, Sandhu J, Lee YW, Cameron RG, Hendler A, Vallis K and Gariépy J: A comparison of EGF and MAb 528 labeled with ^{111}In for imaging human breast cancer. J Nucl Med *41*: 903-911, 2000.

10 Torres LA, Perera A, Batista JF, Hernández A, Crombet T, Ramos M, Neninger E, Pérez M, Sánchez EL, Romero S, Aguilar V, Coca MA and Iznaga-Escobar N: Phase I/II clinical trial of the humanized anti-EGF-r monoclonal antibody h-R3 labeled with ^{99m}Tc in patients with tumour of epithelial origin. Nucl Med Commun *26*: 1049-1057, 2005.

11 Wang X, Zhu J, Zhao P, Jiao Y, Xu N, Grabinski T, Liu C, Miranti CK, Fu T and Cao BB: *In vitro* efficacy of immuno-chemotherapy with anti-EGFR human Fab-taxol conjugate on A431 epidermoid carcinoma cells. Cancer Biol Ther *6*: 980-987, 2007.

12 Hay RV, Cao B, Skinner RS, Su Y, Zhao P, Gustafson MF, Teh BT, Knudsen BS, Resau JH, Shen S, Waters DJ, Gross MD and Vande Woude GF: Nuclear imaging of Met-expressing human and canine cancer xenografts with radiolabeled monoclonal antibodies. Clin Cancer Res *11*: 7064s-7069s, 2005.

13 Carter T, Sterling-Levis K, Ow K, Doughty L, Hattarki M, Shapira D, Hewish D, Kortt AA and Russell PJ: Biodistributions of intact monoclonal antibodies and fragments of BLCA-38, a new prostate cancer directed antibody. Cancer Immunol Immunother *53*: 533-542, 2004.

14 Haigler H, Ash JF, Singer SJ and Cohen S: Visualization by fluorescence of the binding and internalization of epidermal growth factor in human carcinoma cells A-431. Proc Natl Acad Sci USA *75*: 3317-3321, 1978.

15 Vincenzi B, Santini D, Rabitti C, Coppola R, Beomonte Zobel B, Trodella L and Tonini G: Cetuximab and irinotecan as third-line therapy in advanced colorectal cancer patients: a single-centre phase II trial. Br J Cancer *94*: 792-797, 2006.

16 Chung KY, Shia J, Kemeny NE, Shah M, Schwartz GK, Tse A, Hamilton A, Pan D, Schrag D, Schwartz L, Klimstra DS, Fridman D, Kelsen DP and Saltz LB: Cetuximab shows activity in colorectal cancer patients with tumors that do not express the epidermal growth factor receptor by immunohistochemistry. J Clin Oncol *23*: 1803-1810, 2005.

17 Pnwar P, Iznaga-Escobar N, Mishra P, Srivastava V, Sharma RK, Chandra R and Mishra AK: Radiolabeling and biological evaluation of DOTA-Ph-Al derivative conjugated to anti-EGFR antibody for EGFR/R3 for targeted tumor imaging and therapy. Cancer Biol Ther *4*: 854-860, 2005.

18 Panousis C, Rayzman VM, Johns TG, Renner C, Liu Z, Cartwright G, Lee FT, Wang D, Gan H, Cao D, Kypridis A, Smyth FE, Brechbiel MW, Burgess AW, Old LJ and Scott AM: Engineering and characterisation of chimeric monoclonal antibody 806 (ch806) for targeted immunotherapy of tumors expressing de2-7 EGFR or amplified EGFR. Br J Cancer *92*: 1069-1077, 2005.

19 van Dongen GA, Visser GW and Vrouenraets MB: Photosensitizer-antibody conjugates for detection and therapy of cancer. Adv Drug Deliv Rev *56*: 31-52, 2004.

20 Friedländer E, Barok M, Szöllosi J and Vereb G: ErbB-directed immunotherapy: antibodies in current practice and promising new agents. Immunol Lett *116*: 126-140, 2008.

21 Jiao Y, Zhao P, Zhu J, Grabinski T, Feng Z, Guan X, Skinner RS, Gross MD, Hay RV, Tachibana H and Cao B: Construction of human naïve Fab library and characterization of anti-Met Fab fragment generated from the library. Mol Biotechnol *31*: 41-54, 2005.

22 Nordberg E, Orlova A, Friedman M, Tolmachev V, Stahl S, Nilsson FY, Glimelius B and Carlsson J: *In vivo* and *in vitro* uptake of ^{111}In, delivered with the affibody molecule (ZEGFR: 955)2, in EGFR-expressing tumour cells. Oncol Rep *19*: 853-857, 2008.

23 Huang L, Gainkam LO, Caveliers V, Vanhove C, Keyaerts M, De Baetselier P, Bossuyt A, Revets H and Lahoutte T: SPECT imaging with ^{99m}Tc-labeled EGFR-specific nanobody for *in vivo* monitoring of EGFR expression. Mol Imaging Biol *10*: 167-175, 2008.

24 Goldenberg DM: Targeted therapy of cancer with radiolabeled antibodies. J Nucl Med *43*: 693-713, 2002.

Received May 10, 2009
Revised July 27, 2009
Accepted August 31, 2009